**Astronomy & Astrophysics**

# Electron density in the quiet solar coronal transition region from SoHO/SUMER measurements of S VI line radiance and opacity

E. Buchlin and J.-C. Vial

Institut d'Astrophysique Spatiale, CNRS & Université Paris Sud, Orsay, France
e-mail: eric.buchlin@ias.fr

**ABSTRACT**

*Context.* The steep temperature and density gradients that are measured in the coronal transition region challenge the model interpretation of observations.

*Aims.* We derive the average electron density $\langle n_e \rangle$ in the region emitting the S VI lines. We use two different techniques, which allow us to derive linearly-weighted (opacity method) and quadratically-weighted (emission measure method) electron density along the line-of-sight, to estimate a filling factor or derive the layer thickness at the formation temperature of the lines.

*Methods.* We analyze SoHO/SUMER spectroscopic observations of the S VI lines, using the center-to-limb variations in radiance, the center-to-limb ratios of radiance and line width, and the radiance ratio of the 93.3–94.4 nm doublet to derive the opacity. We also use the emission measure derived from radiance at disk center.

*Results.* We derive an opacity $\tau_0$ at S VI 93.3 nm line center of the order of 0.05. The resulting average electron density $\langle n_e \rangle$, under simple assumptions concerning the emitting layer, is $2.4 \times 10^{16}$ m$^{-3}$ at $T = 2 \times 10^5$ K. This value is higher than (and inconsistent with) the values obtained from radiance measurements ($2 \times 10^{15}$ m$^{-3}$). The last value corresponds to an electron pressure of $10^{-2}$ Pa. Conversely, taking a classical value for the density leads to a too high value of the thickness of the emitting layer.

*Conclusions.* The pressure derived from the emission measure method compares well with previous determinations. It implies a low opacity of between $5 \times 10^{-3}$ and $10^{-2}$. It remains unexplained why a direct derivation leads to a much higher opacity, despite tentative modeling of observational biases. Further measurements in S VI and other lines emitted at a similar temperature should be completed, and more realistic models of the transition region need to be used.

**Key words.** Sun: atmosphere – Sun: transition region – Sun: UV radiation

## 1. Introduction

In the simplest description of the solar atmosphere as a series of concentric spherical layers of plasma at different densities and temperatures, the transition region (hereafter TR) between the chromosphere and the corona is the thin interface between the high-density and low-temperature chromosphere (a few $10^{16}$ m$^{-3}$ hydrogen density at about $10^4$ K) and the low-density and high-temperature corona (about $10^{14}$ m$^{-3}$ at $10^6$ K). The variation in temperature $T$ and electron number density $n_e$ was mostly derived from the modelling of this transition region, where radiative losses are balanced by thermal conduction (e.g. Mariska 1993; Avrett & Loeser 2008).

Measurements of the electron density usually depend on either estimation of the emission measure or line ratios. On the one hand, using absolute line radiances, the emission measure (EM) and differential emission measure (DEM) techniques provide $\langle n_e^2 \rangle$ at the formation temperature of a line (or as a function of temperature, if several lines covering a range of temperatures are measured). On the other hand, the technique of line radiance ratios provides a wealth of values of $n_e$ (Mason 1998) with the assumption of uniform density along the line-of-sight, and with an accuracy that is limited by the accuracy of the two respective radiance measurements: a 15% uncertainty in the line radiance measurement typically leads to a 30% uncertainty in the line ratio and then about a factor 3 of uncertainty in the density.

However, for a given pair of lines, this technique only works for a limited range of densities. We add that the accuracy is also limited by the precision of atomic physics data.

Here we also propose to use the concept of opacity (or optical thickness) to derive the population of the low (actually the ground) level $i$ of a given transition $i \rightarrow j$, and then the electron density. At a given wavelength, the opacity of a column of plasma corresponds to the sum of the absorption coefficients of photons by the individual ions in the column. The opacity can be derived by different complementary techniques (Dumont et al. 1983), if many measurements are available with spatial (preferably center-to-limb) information. This is the case in a full-Sun observation program by the SoHO/SUMER UV spectro-imager (Wilhelm et al. 1995; Peter 1999; Peter & Judge 1999) run in 1996. In particular, because of a specific "compressed" mode, a unique dataset of 36 full-Sun observations in S VI lines was obtained, enabling that it is possible at the same time to derive $\langle n_e \rangle$ from opacity measurements and $\langle n_e^2 \rangle$ from line radiance measurements (via the EM).

We already used this data set to derive properties about the turbulence in the TR (Buchlin et al. 2006). We note here that, in contrast to Peter (1999), Peter & Judge (1999), and Buchlin et al. (2006), we are not interested in the resolved directed velocities or in the non-thermal velocities but in the line radiances, peak spectral radiances, and widths. We also note that, along with the

**Table 1.** Spectral lines present in the data sets, with parameters computed by CHIANTI and given by previous observations.

| | | CHIANTI[a] | | | Curdt et al. (2001) | |
|---|---|---|---|---|---|---|
| ion | transition $j \rightarrow i$ | $\log T_{max}$ (K) | wavelength (Å) | radiance[b] | wavelength (Å) | peak radiance[b] |
| S VI | $2p^6\, 3p\; ^2P_{3/2} \rightarrow 2p^6\, 3s\; ^2S_{1/2}$ | 5.3 | 933.3800 | $3.81 \times 10^{-3}$ | 933.40 | 0.57 |
| Ly $\varepsilon$ | $6p\; ^2P_{3/2} \rightarrow 1s\; ^2S_{1/2}$ | — | — | — | 937.80 | 1.07 |
| Si VIII | $2s^2\, 2p^3\; ^2P_{3/2} \rightarrow 2s^2\, 2p^3\; ^4S_{3/2}$ | 5.9 | 944.4670 | $5.24 \times 10^{-3}$ | 944.34 | 0.14 |
| S VI | $2p^6\, 3p\; ^2P_{1/2} \rightarrow 2p^6\, 3s\; ^2S_{1/2}$ | 5.3 | 944.5240 | $1.91 \times 10^{-3}$ | 944.55 | 0.29 |

[a] Using the "Arnaud & Raymond" ionization fractions file, the "Sun coronal" abundance file and the "quiet Sun" DEM file. CHIANTI does not include data for the Hydrogen lines (Ly $\varepsilon$ in particular).
[b] Radiances are given in $W\,m^{-2}\,sr^{-1}$, and peak spectral radiances are given in $W\,m^{-2}\,sr^{-1}\,nm^{-1}$.

modelling work of Avrett & Loeser (2008), we do not attempt to differentiate between network and internetwork, which can be a difficult task at the limb, and aim to precisely determinate the properties of an average TR.

This paper is organized as follows: we first present the data set that use, we then we determine opacities and radiances of S VI 93.3 nm, we derive two determinations of density in the region emitting the S VI 93.3 nm line, we discuss the disagreement between the two determinations (especially possible biases), and finally we conclude.

## 2. Data

### 2.1. Data sets

We use the data from a SoHO/SUMER full-Sun observation program in S VI 93.3 nm, S VI 94.4 nm, and Ly $\varepsilon$ designed by Philippe Lemaire. The spectra, obtained with detector A of SUMER and for an exposure time of 3 s, were not sent to the ground (except for context spectra) but 5 parameters ("moments") of 3 lines were computed on board for each position on the Sun: (1) peak spectral radiance; (2) Doppler shift; and (3) width of the line S VI 93.3 nm; (4) line radiance (integrated spectral radiance) of the line Ly $\varepsilon$ 93.8 nm; (5) line radiance of the line S VI 94.4 nm, which is likely to be blended with Si VIII.

The detailed characteristics of these lines can be found in Table 1. A list of the 36 observations of this program completed throughout year 1996, close to solar minimum, can be found in Table 1 of Buchlin et al. (2006). These original data constitute the main data set that we use in this paper, hereafter DS1. They are complemented by a set of 22 context observations from the same observing program, which we use when we need the full profiles of the spectral lines close to disk center: the full SUMER detector ($1024 \times 360$ pixels) was recorded at a given position on the Sun at less than 40 arcsec from disk center and with an exposure time of 300 s. This data was calibrated using the Solar Software procedure `sum_read_corr_fits` (including correction of the flat field, as measured on 23 September 1996, and of distortion), and it will hereafter be referred to as DS2.

### 2.2. Averages of the data as a function of distance to disk center

To obtain averages of the radiances in data set DS1 as a function of the radial distance $r$ to the disk center, and, as a function of $\mu$, the cosine of the angle between the normal to the solar "surface" and the line-of-sight, we apply the following method, assuming that the Sun is spherical:

– We detect the limb automatically by finding the maximum of the S VI 93.3 nm radiance at each solar-$y$ position in two
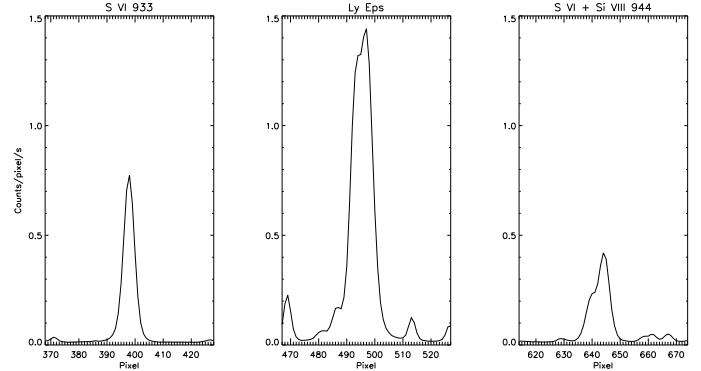


**Fig. 1.** Raw line profiles from the context spectrum taken on 4 May 1996 at 07:32 UT at disk center with an exposure time of 300 s. The profiles are averaged over pixels 50 to 299 along the slit ($1 \times 300$ arcsec, detector A), with no prior destretching of the data.

detection windows in the solar-$x$ direction, corresponding to the approximate expected position of the limb. This means that the limb is found in a TR line and is approximately 3 arcsec above the photosphere. However, this is the relevant limb position for the geometry of the S VI 93.3 nm emission region.

– We fit these limb positions to arcs of a circle described by $x(y)$ functions, and we derive the true position $(a, b)$ of the solar disk center in solar coordinates $(x, y)$ given by SUMER, and the solar radius $R_\odot$, which changes as a function of the time of year due to the eccentricity of SoHO's orbit around the Sun. The solar radius is evaluated for the observed wavelength of 93.3 nm.

– We exclude zones corresponding to active regions, because we attempt to obtain properties of the TR in the quiet Sun.

– For each of the remaining pixels, we derive values of the radial distance $r = \sqrt{(x-a)^2 + (y-b)^2}$ to disk center and of $\mu = \sqrt{1 - (r/R_\odot)^2}$.

– We compute the averages of each moment (radiances and widths) in bins of both $r/R_\odot$ and $1/\mu$.

The resulting averages as a function of $r/R_\odot$ and of $1/\mu$ are plotted in Fig. 2 except for the S VI 93.3 nm Doppler shift, which will not be used in this paper. The radiances are approximately linear functions of $1/\mu$ for small $1/\mu$, as expected for optically thin lines in a plane-parallel geometry. This behavior supports the assumption of a "mean" plane-parallel transition region, at least for $1/\mu < 10$ or $\theta < 84°$.
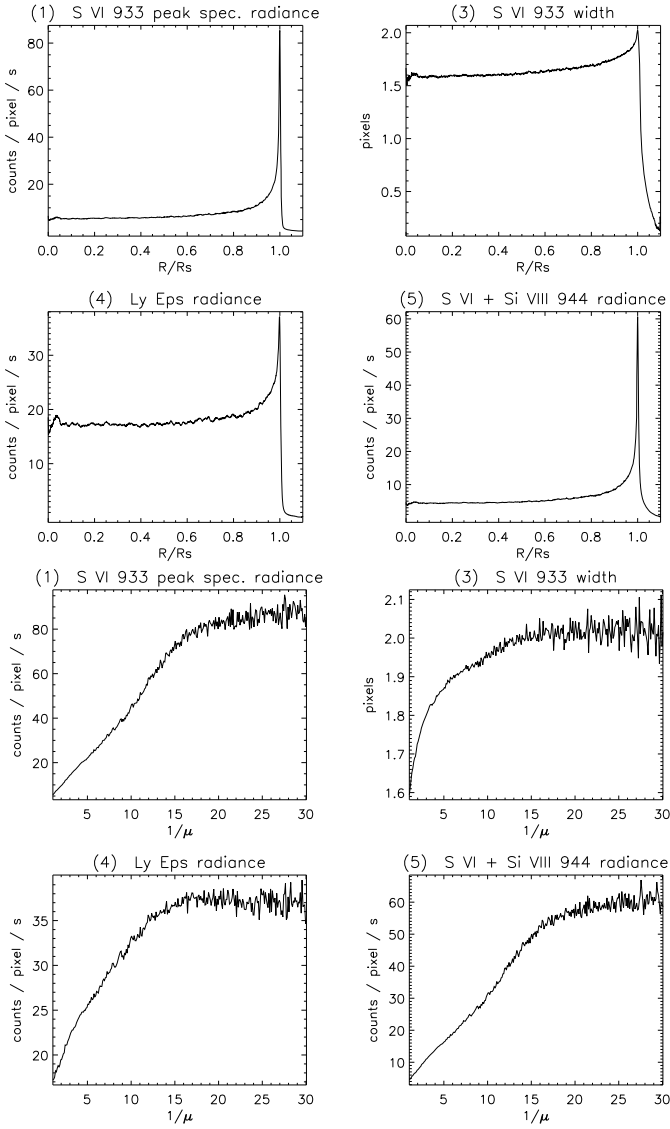
**Fig. 2.** Average of the data as a function of $r/R_\odot$ (*top panels*) and as a function of $1/\mu$ (*bottom panels*).

## 3. Determination of opacities

### 3.1. Using center-to-limb variations

We follow the method A proposed by Dumont et al. (1983). Assuming that the TR is spherically symmetric and can be assumed to be plane-parallel when not seen too close to the limb, that the lines are optically thin, and that the source function $S$ is constant in the region where the line is formed[1], the spectral radiance is:

$$I_0(\mu) = S\left(1 - \exp(-\tau_0/\mu)\right) \tag{1}$$

where the subscript 0 is for the line center and $\tau$ is the opacity of the emitting layer at disk center. We then have that:

$$I_0(\mu) = I_0(1)\frac{1 - \exp(-\tau_0/\mu)}{1 - \exp(-\tau_0)} \tag{2}$$

and a fit of the observed $I_0(\mu)$ by this function, where $I_0(1)$ and $\tau_0$ are parameters[2], provides an estimate of $\tau_0$.

[1] We release this assumption in Sect. 5.
[2] Note that, in contrast to Dumont et al. (1983), we consider $I_0(1)$ as an additional parameter. This is because by doing so, we avoid the

For the lines for which only the line radiance $E$ is known (S VI 94.4 nm and Ly $\varepsilon$), we need to fit the following function, where $\tau_0$ and $E(1)$ are parameters[3]:

$$E(\mu) = E(1)\frac{\int_\mathbb{R}\left(1 - \exp\left(-\frac{\tau_0}{\mu}\,e^{-u^2}\right)\right)du}{\int_\mathbb{R}\left(1 - \exp\left(-\tau_0\,e^{-u^2}\right)\right)du}\,. \tag{3}$$

This expression is derived from Dumont et al. (1983) and assumes a Doppler absorption profile $\exp(-u^2)$ with $u = \Delta\lambda/\Delta\lambda_D$. Here, in contrast to the peak spectral radiance ratio, the function and its derivatives with respect to $\tau_0$ and $E(1)$ cannot be computed analytically, but must be estimated numerically; this is achieved by a fast method, using a Taylor expansion of the outermost exponential of both the numerator and denominator of Eq. (3).

These theoretical functions of $\mu$ are then plotted for different values of the parameter $\tau_0$ over the observations in Fig. 3, for all three lines (either for the peak spectral radiance or the line radiance, depending on the data). We performed a non-linear least squares fit with the Levenberg-Marquardt algorithm as implemented in the Interactive Data Language (IDL) to estimate the parameter $\tau_0$. The uncertainties in each point of the $E(\mu)$ or $I(\mu)$ functions (an average of $N_d$ pixels) that we take as input to the fitting procedure come mainly from the possible presence of coherent structures such as bright points: the number of possible structures is of the order $N_d/N_s$, where $N_s$ is the size of these structures (we assume $N_s = 100$ pixels), and then the uncertainty in $I$ or $E$ is $\sigma/\sqrt{N_d/N_s}$ where $\sigma$ is the standard deviation of the data points (in each pixel of a $1/\mu$ bin). Compared to this uncertainty, the photon noise is negligible.

The results of the fits for the interval $1/\mu \in [1, 5]$ are shown in Fig. 3: as far as $\tau_0$ is concerned, they are 0.113 for moment (1) (S VI 93.3 nm peak spectral radiance) and 0.244 for moment (5) (S VI 94.4 nm radiance, blended with Si VIII). The approximations that we used in writing Eq. (1) are invalid for the optically thick Ly $\varepsilon$ line, which should explain the poor fit. On the other hand, these approximations are valid for both the S VI lines, as long as $1/\mu$ is small enough. For large $1/\mu$, there is an additional uncertainty resulting from the determination of the limb.

These results are sensitive to the limb fitting: a $10^{-3}$ relative error in the determination of the solar radius leads to a $7 \times 10^{-2}$ relative error in $\tau_0$. Since $10^{-3}$ is a conservative upper limit to the error in the radius from the limb fitting, we can consider $7 \times 10^{-2}$ to be a conservative estimate of the relative error in $\tau_0$ resulting from the limb fitting.

### 3.2. Using center-to-limb ratios of S VI 93.3 nm width and radiance

The variation with position of the S VI 93.3 nm line width (see Fig. 2) can be interpreted as an opacity saturation of the S VI 93.3 nm line at the limb, and method B of Dumont et al. (1983) can then be applied. This method relies on the measurement of the ratio $d = \Delta\lambda_l^*/\Delta\lambda_c^*$ of the FWHM at the limb and the disk center: the optical thickness at line center $t_0$ at the limb is given by solving

$$2\left(1 - \exp\left(-t_0\,e^{-d^2\ln 2}\right)\right) = 1 - \exp(-t_0), \tag{4}$$

sensitivity of $I_0(1)$ to structures close to disk center, and because the first data bin *starts* at $1/\mu = 1$ instead of being centered on $1/\mu = 1$.
[3] We take here $E(1)$ as a parameter for the same reason as we did before for $I_0(1)$.
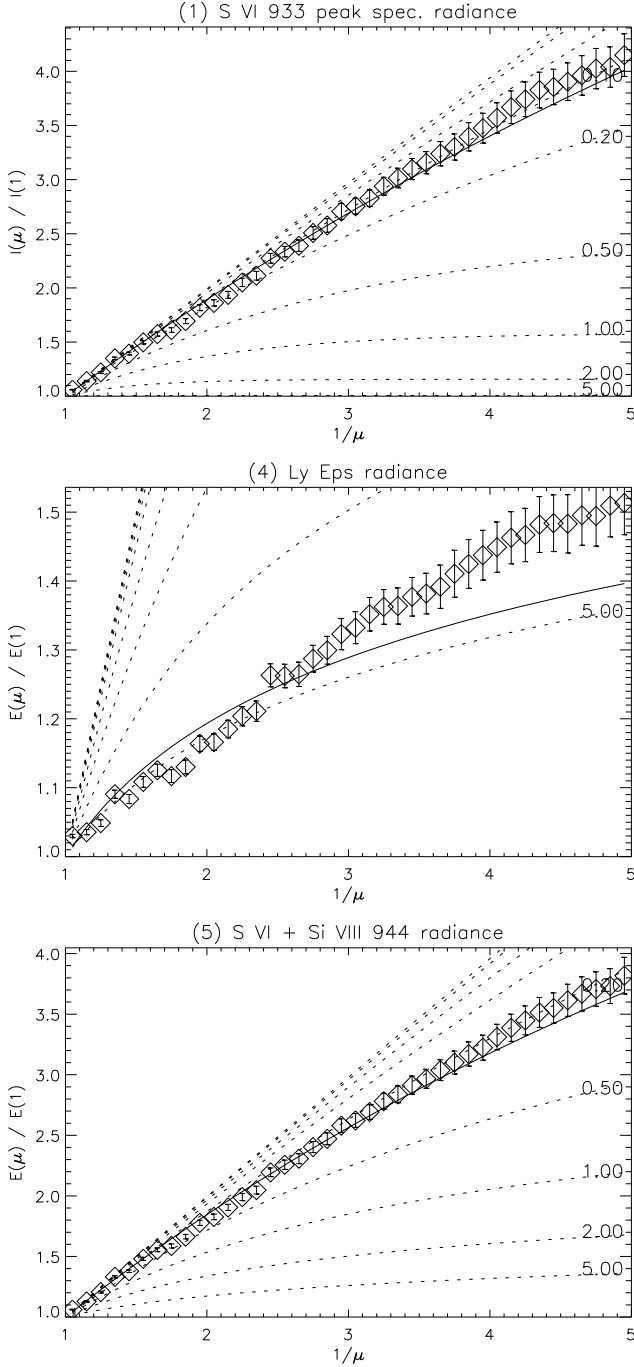
**Fig. 3.** Diamonds: average profiles of the radiance data (moments 1, 4 and 5) as a function of $1/\mu$, normalized to their values at disk center. Dotted lines: theoretical profiles for different values of $\tau_0$. Plain lines: fits of the theoretical profiles to the data, giving the values for $\tau_0$: 0.113 for (1) and 0.244 for (5). The fit for Ly $\varepsilon$ is bad because this line is optically thick.

which is Eq. (4) of Dumont et al. (1983), where a sign error has been corrected, and the opacity at line center $\tau_0$ is then given by solving

$$\frac{I_0(\mu = 1)}{I_0(\mu = 0)} = \frac{1 - \exp(-\tau_0)}{1 - \exp(-t_0)}. \tag{5}$$

Using the full-Sun S VI 93.3 nm compressed data set DS1[4], we measure the ratio $d$ to be 1.274 and $t_0$ to be 1.53. Finally, we use the S VI 93.3 nm peak spectral radiance ratio $I_0(\mu = 1)/I_0(\mu = 0) = 0.062$ to derive $\tau_0 = 0.05$.

### 3.3. Using the S VI 94.4 − 93.3 line ratio

The theoretical dependence of the S VI 94.4 − 93.3 peak radiance line ratio as a function of the line opacities and source functions is

$$K = \frac{I_{0,933}}{2 I_{0,944}} = \frac{S_{933}}{2 S_{944}} \cdot \frac{1 - \exp(-\tau_{0,933})}{1 - \exp(-\tau_{0,944})}. \tag{6}$$

For this doublet, we assume $S_{933} = S_{944}$ and $\tau_{0,933} = 2\tau_{0,944}$ (because the oscillator strengths are in the proportion $f_{933} = 2f_{944}$). Then $K$ reduces to

$$K = \frac{1}{2} \cdot \frac{1 - \exp(-\tau_{0,933})}{1 - \exp(-\tau_{0,933}/2)} = \frac{1 + \exp(-\tau_{0,933}/2)}{2} \tag{7}$$

and we derive $\tau_{0,933}$ from the observed value of $K$ to be

$$\tau_{0,933} = -2\ln(2K - 1). \tag{8}$$

The difficulty is that the S VI 94.4 nm line is blended with the Si VIII line. To remove this blend, we analyzed the line profiles available in data set DS2. After averaging the line profiles over the 60 central pixels along the slit, we fitted the S VI 93.3 nm line with a Gaussian and a uniform background, and the S VI 94.4 nm line blend with two Gaussians and a uniform background. We then computed the Gaussian amplitude from these fits for both S VI lines, to measure $I_{0,933}$ and $I_{0,944}$, and then $K$, which we averaged over all observations. From this method, we inferred that $\tau_{0,933} = 0.089$.

The same kind of method could in theory be used for the S VI 94.4 − 93.3 line radiance ratio

$$K = \frac{E_{933}}{2 E_{944}} = \frac{S_{933}}{2 S_{944}} \frac{\int_{\mathbb{R}} \left(1 - \exp\left(-\tau_{0,933} \, e^{-u^2}\right)\right) du}{\int_{\mathbb{R}} \left(1 - \exp\left(-\tau_{0,944} \, e^{-u^2}\right)\right) du} \tag{9}$$

with, again, $S_{933} = S_{944}$ and $\tau_{0,933} = 2\tau_{0,944}$. As for method A, the integral makes it necessary to invert this function of $\tau_{0,933}$ numerically, to recover $\tau_{0,933}$ for a given observed value of $K$. Since $K$ decreases as a function of $\tau_{0,933}$, this is possible by a simple dichotomy. However, the average $K$ from the observations is greater than 1, which makes it impossible to invert the function and obtain a value for $\tau_0$.

### 3.4. Discussion about opacity determination

It is clear that the three methods provide different values of the opacity at disk center. We confirm the result of Dumont et al. (1983), obtained in different lines, by which the method of center-to-limb ratios of width and radiance (Sect. 3.2, or method B in Dumont et al. 1983) provides the smallest value of the opacity. As mentioned by these authors, the center-to-limb variation method (Sect. 3.1, or method A) overestimates the opacity for different reasons described in Dumont et al. (1983), including the curvature of the layers close to the limb and their roughness. The method of line ratios (Sect. 3.3, or method C)

---

[4] Although not obvious from the data headers, moment (3) corresponds to the deconvoluted FWHM of S VI 93.3 nm, as confirmed by comparing with the width obtained from the full profiles in data set DS2 and deconvoluted using the Solar Software procedure `con_width_4`.

also provides larger values of the opacity, although free from geometrical assumptions; Dumont et al. (1983) interpret them as resulting from a difference between the source functions of the lines of the doublet.

This does not mean that there are no additional biases. For instance, we adopted a constant Doppler width from center to limb; this is incorrect since, at the limb, the observed layer is at higher altitude, where the temperature and turbulence are higher than in the emitting layer as viewed at disk center. Consequently, the excessive line width is wrongly interpreted as only an opacity effect. However, it seems improbable that a 27.4% increase in Doppler width from center to limb can be interpreted entirely in terms of temperature (because of the square-root temperature variation in Doppler width) and turbulence (since the emitting layer is – a posteriori – optically not very thick).

## 4. First estimates of densities

### 4.1. Densities using the opacities

The line-of-sight opacity at line center of the S VI 93.3 nm line is given by

$$\tau_0 = \int k_{\nu_0} \, n_{\mathrm{S\,VI},i}(s) \, \mathrm{d}s, \tag{10}$$

where the integration is along the line-of-sight. The variable $n_{\mathrm{S\,VI},i}$ is the numerical density of S VI in its level $i$, which can be written as

$$n_{\mathrm{S\,VI},i} = \frac{n_{\mathrm{S\,VI},i}}{n_{\mathrm{S\,VI}}} \frac{n_{\mathrm{S\,VI}}}{n_{\mathrm{S}}} \, \mathrm{Abund(S)} \frac{n_{\mathrm{H}}}{n_{\mathrm{e}}} n_{\mathrm{e}}, \tag{11}$$

where $\mathrm{Abund(S)} = n_{\mathrm{S}}/n_{\mathrm{H}}$ is the sulfur abundance in the corona ($10^{-4.73}$ according to the CHIANTI database, Dere et al. 1997; Landi et al. 2006), $n_{\mathrm{S\,VI},i}/n_{\mathrm{S\,VI}}$ is the proportion of S VI at level $i$, $n_{\mathrm{S\,VI}}/n_{\mathrm{S}}$ is the ionization fraction (known as a function of temperature), and $n_{\mathrm{H}}/n_{\mathrm{e}} = 0.83$ is constant in a fully ionized medium such as the upper transition region. In this work, $i$ is the ground state $i = 1$, and since in this region $n_{\mathrm{S\,VI},1}/n_{\mathrm{S\,VI}}$ is very close to 1, we neglect this term from now. The variable $k_{\nu_0}$ is the absorption coefficient at line center frequency $\nu_0$ for each S VI ion, given by

$$k_{\nu_0} = \frac{h\nu_0}{4\pi} B_{ij} \frac{1}{\sqrt{\pi}\,\Delta\nu_D}, \tag{12}$$

where $B_{ij}$ is the Einstein absorption coefficient for the transition $i \to j$ (i.e., $2\mathrm{p}^6\,3\mathrm{s}\,{}^2\mathrm{S}_{1/2} \to 2\mathrm{p}^6\,3\mathrm{p}\,{}^2\mathrm{P}_{3/2}$) at $\lambda_0 = 93.3$ nm, and integration over a Gaussian Doppler shift distribution was completed ($\Delta\nu_D$ is the Doppler width in frequency). Using

$$B_{ij} = \frac{g_j}{g_i} B_{ji} = \frac{g_j}{g_i} \frac{A_{ji}}{2\,h\nu_0^3/c^2} \tag{13}$$

with $g_j/g_i = 2$ and $\lambda_0 = c/\nu_0$, this infers that

$$k_{\nu_0} = \frac{\lambda_0^4 A_{ji}}{4\pi^{3/2} c\,\Delta\lambda_D} \tag{14}$$

Finally, for an emitting layer of thickness $\Delta s$ and average electron density $\langle n_{\mathrm{e}} \rangle$, we have

$$\tau_0 = \frac{\lambda_0^4 A_{ji}}{4\pi^{3/2} c\,\Delta\lambda_D} \frac{n_{\mathrm{S\,VI}}}{n_{\mathrm{S}}} \, \mathrm{Abund(S)} \frac{n_{\mathrm{H}}}{n_{\mathrm{e}}} \langle n_{\mathrm{e}} \rangle \, \Delta s. \tag{15}$$

Taking $\tau_0 = 0.05$, we derive $\langle n_{\mathrm{e}} \rangle \Delta s = 4.9 \times 10^{21}$ m$^{-2}$. Then, with $\Delta s = 206$ km (the altitude interval corresponding to the FWHM of the S VI 93.3 nm contribution function $G(T)$ as computed by CHIANTI), this infers that $\langle n_{\mathrm{e}} \rangle = 2.4 \times 10^{16}$ m$^{-3}$.

### 4.2. Squared densities using the contribution function

The average S VI 93.3 nm line radiance at disk center obtained from data set DS2 (excluding the 5% higher values not considered to be part of the quiet Sun) is $E = 1.4 \times 10^{-2}$ W m$^{-2}$ sr$^{-1}$ (compared to the value $3.81 \times 10^{-3}$ given by CHIANTI with a quiet Sun DEM – see Table 1). This can be used to estimate $\langle n_{\mathrm{e}}^2 \rangle \Delta s$ in the emitting region of thickness $\Delta s$, since

$$E = \int G(T(s)) \, n_{\mathrm{e}}^2(s) \, \mathrm{d}s \approx G(\langle T \rangle) \, \langle n_{\mathrm{e}}^2 \rangle \, \Delta s, \tag{16}$$

where $G(T)$ is the contribution function, the integral is evaluated along the line-of-sight, and we assume that $\tau_0 \ll 1$. We take the average temperature in the emitting region to be $\langle T \rangle = T_{\max} = 10^{5.3}$ K, and, for densities of the order of $10^{16}$ m$^{-3}$, the `gofnt` function of CHIANTI infers $G(\langle T \rangle) = 1.8 \times 10^{-37}$ W m$^3$ sr$^{-1}$. We finally derive

$$\langle n_{\mathrm{e}}^2 \rangle \Delta s = 8.4 \times 10^{35} \text{ m}^{-5}. \tag{17}$$

Again for $\Delta s = 206$ km, we obtain $\langle n_{\mathrm{e}} \rangle_{\mathrm{rms}} = 2.0 \times 10^{15}$ m$^{-3}$. Assuming an uncertainty of 20% in $E$, the uncertainty in $\langle n_{\mathrm{e}} \rangle_{\mathrm{rms}}$ should be 10% for a given $\Delta s$.

## 5. Discussion of biases in the method

At the start of this work, one of our aims was to determine a filling factor[5]

$$f = \frac{\langle n_{\mathrm{e}} \rangle^2}{\langle n_{\mathrm{e}}^2 \rangle} \tag{18}$$

in the S VI-emitting region. This initial objective needs to be reviewed, because we obtain $f = 144$, an impossible value as it is more than 1. Our values of densities can be compared with the density at $\log T = 5.3$ in the Avrett & Loeser (2008) model ($1.7 \times 10^{15}$ m$^{-3}$): our value of $\langle n_{\mathrm{e}} \rangle$ is an order of magnitude higher, while $\langle n_{\mathrm{e}} \rangle_{\mathrm{rms}} = \sqrt{\langle n_{\mathrm{e}}^2 \rangle}$ is about the same (while it should be higher than $\langle n_{\mathrm{e}} \rangle$). Our value of intensity is compatible with average values from other sources, such as Del Zanna et al. (2001) (see their Fig. 1).

Given the same measurements of $\tau_0$ and $E$, one can instead assume of a filling factor $f \in [0, 1]$ and infer $\Delta s$ to be

$$\Delta s = \frac{1}{f} \cdot \frac{(\langle n_{\mathrm{e}} \rangle \, \Delta s)^2}{\langle n_{\mathrm{e}}^2 \rangle \, \Delta s}, \tag{19}$$

where the numerator and denominator of the second quotient in the product shown are determined from Eqs. (15) and (16) respectively. With the values from Sect. 4, this gives $\Delta s > 29$ Mm $= 0.04\,R_\odot$, a value much larger than expected.

In any case, there seems to be some inconsistencies for $\log T = 5.3$ between on the one hand our new observations of opacities, and on the other hand transition region models and observations of intensities. We now propose to discuss the possible sources of these discrepancies, while releasing, when needed, some of the simplistic assumptions we have so far made.

### 5.1. Assumption of a uniform emitting layer

#### 5.1.1. Bias due to this assumption

When computing the average densities from the S VI 93.3 nm opacity and radiance, we assumed a uniform emitting layer at

---

[5] We explain this definition of the filling factor in Appendix A.

the temperature of maximum emission and of thickness $\Delta s$ given by the width of contribution function $G(T)$. However, the different dependences of the electron density in Eqs. (10) and (16) – the first is linear while the second is quadratic – means that the slope of the $n_e(s)$ function affects the weights on the integrals of Eqs. (10) and (16) differently: a bias, different for $\tau_0$ and $E$, can be expected, and here we explore this effect starting from the Avrett & Loeser (2008) model, which has the merit of giving average profiles of temperature and density (among other variables) as a function of altitude $s$.

**Opacity.** Using the Avrett & Loeser (2008) profiles and atomic physics data, we derive $\tau_0 = 0.008$. Then, using the same simplistic method as for observations (still with a uniform layer of thickness $\Delta s = 206$ km), we obtain $\langle n_e \rangle = 2.4 \times 10^{15}$ m$^{-3}$, a value only 40% higher than the density at $\log T = 5.3$ in this model ($1.7 \times 10^{15}$ m$^{-3}$).

**Radiance.** Using the same Avrett & Loeser (2008) profiles and the CHIANTI contribution function $G(T)$, we derive $E = 1.3 \times 10^{-2}$ W m$^{-2}$ sr$^{-1}$. Then, using the same simplistic method as for observations, we obtain $\langle n_e \rangle_{\rm rms} = 1.9 \times 10^{15}$ m$^{-3}$, a value 12% higher than the density at $\log T = 5.3$ in this model.

We see then that the assumption of a uniform emitting layer has a bias towards high densities, which is stronger for the opacity method than for the radiance method. A filling factor computed from these values would be $f = 1.5$, while it was assumed to be 1 when computing $\tau_0$ and $E$ from the Avrett & Loeser (2008) model: this can be one of the reasons for our too high observed filling factor.

This differential bias acts surprisingly because, according to the $n_e^2$ term in Eq. (16) one would expect the bias to be stronger for $E$ than for $\tau_0$; however, it can be understood by comparing the effective temperatures for $\tau_0$ and $E$, which are respectively

$$T_{\text{eff},\tau_0} = \frac{\int T(s)\, n_e(s)\, K(T(s))\, {\rm d}s}{\int n_e(s)\, K(T(s))\, {\rm d}s} = 10^{5.38}\ \text{K, and} \qquad (20)$$

$$T_{\text{eff},E} = \frac{\int T(s)\, n_e^2(s)\, G(T(s))\, {\rm d}s}{\int n_e^2(s)\, G(T(s))\, {\rm d}s} = 10^{5.40}\ \text{K,} \qquad (21)$$

where $K(T) = k_{\nu_0}(T)\, n_{\rm S\,VI}/n_e$, while $T(s)$ and $n_e(s)$ are from Avrett & Loeser (2008). The higher effective temperature for $E$ than for $\tau_0$ means that the bias is more affected by the respective shapes of the high-temperature wings of $G(T)$ and $K(T)$ than by the exponent of $n_e$ in the integrals of Eqs. (12) and (16).

It can be pointed out that the difference between the $K(T)$ and $G(T)$ kernels is present because $G(T)$ (unlike $K(T)$) takes into account not only the ionization equilibrium of S VI, but also the collisions from $i$ to $j$ levels of S VI ions.

### 5.1.2. Releasing this assumption: a tentative estimate of the density gradient around $\log T = 5.3$

In Sect. 5.1.1 we have demonstrated that the radiance computed with the Avrett & Loeser (2008) profiles and the CHIANTI contribution function $G(T)$ is a factor of 3 higher than the radiance computed directly by CHIANTI using the standard quiet Sun DEM (see Table 1). This is because the DEM computed from the temperature and density profiles of the Avrett & Loeser (2008)
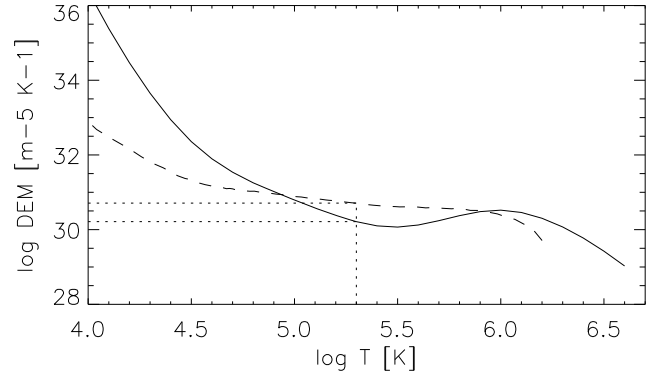
**Fig. 4.** Quiet Sun standard DEM from CHIANTI (plain line) and DEM computed from the Avrett & Loeser (2008) temperature and density profiles dashed lines. The dotted lines represent the DEMs for $\log T = 5.3$, the maximum emission temperature of the S VI lines.

model differs from the CHIANTI DEM[6], as can be seen in Fig. 4. In particular, the Avrett & Loeser (2008) DEM is missing the dip around $\log T = 5.5$ inferred from most observations; at $\log T = 5.3$, it is a factor of 3 higher than the CHIANTI quiet Sun DEM.

We model the upper transition region locally around $\log T_0 = 5.3$ and $s_0 = 2.346$ Mm (chosen because $T(s_0) = T_0$ in the Avrett & Loeser 2008 model) by a vertically stratified plasma at pressure $P_0 = 1.91 n_0 k_B T_0$ (we consider a fully ionized coronal plasma) and

$$\frac{T(s)}{T_0} = \frac{n_0}{n_e(s)} = \sqrt{\frac{s - s_T}{s_0 - s_T}} \quad \text{for} \quad s > s_T. \qquad (22)$$

These equations were chosen to provide a good approximation to a transition region, with some symmetry between the opposite curvatures of the variations in $T$ and $n_e$ with altitude. The parameters of this model atmosphere are the pressure $P_0$ and $s_T$ (with $s_T < s_0$), which can be interpreted as the altitude of the base of the transition region. Given the constraint $T(s_0) = T_0$ that we imposed when building the model with $T_0$ and $s_0$ fixed, $s_T$ controls the derivative of $T(s)$ at $s = s_0$, i.e.,

$$T'(s_0) = \frac{T_0}{2(s_0 - s_T)} \quad \text{or} \quad s_T = s_0 - \frac{T_0}{2T'(s_0)}. \qquad (23)$$

In Fig. 5, we plot some temperature profiles from this simple transition region model, for different model parameters $T'(s_0)$ ($P_0$ only affects the scale of $n_e(s)$). For the Avrett & Loeser (2008) model, $P_0 = 8.7 \times 10^{-3}$ Pa and $T'(s_0) = 0.45$ K m$^{-1}$, and the corresponding model profile is also shown.

We propose to use these models along with atomic physics data and the equations in Sect. 4 to compute $\tau_0$ and $E$ as a function of the model parameters $P_0$ and $T'(s_0)$, as shown in Fig. 6. Since the slopes of the level lines differs in the $\tau_0(P_0, T'(s_0))$ and $E(P_0, T'(s_0))$ plots, one would in theory be able to estimate the parameters $(P_0, T'(s_0))$ of the best fit model for the observation of $(\tau_{0,\text{obs}}, E_{\text{obs}})$ by simply finding the crossing between the level lines $\tau_0(P_0, T'(s_0)) = \tau_{0,\text{obs}}$ and $E(P_0, T'(s_0)) = E_{\text{obs}}$.

In practice however, the level lines for our observations of $\tau_0$ and $E$ do not intersect in the range of parameters plotted in Fig. 6, corresponding to realistic values of the parameters. As a consequence, it is impossible to infer from these measurements

---

[6] The reason for this is that the Avrett & Loeser (2008) model is determined from theoretical energy balance and needs further improvement to reproduce the observed DEM (Avrett, private communication).
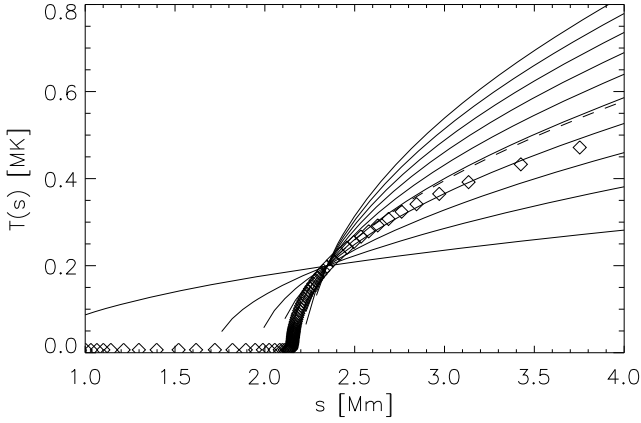
**Fig. 5.** Temperature as a function of altitude in our local transition region simple models around $T_0 = 10^{5.3}$ and $s_0 = 2.346$ Mm. The temperature profile from Avrett & Loeser (2008) is shown with the diamond signs, and the simple model with the same temperature slope is shown with a dashed line.

(from a single spectral line, here S VI 93.3 nm) the temperature slope and the density of the TR around the formation of this line.

If we now extend the range of $T'(s_0)$ to unrealistically low values, a crossing of the level lines can be found below $\log P_0 = -3.5$ and $T'(s_0) = 5$ mK/m. Given the width of $G(T)$ for S VI 93.3 nm, this corresponds to $\Delta s > 20$ Mm, a value consistent with that obtained from Eq. (19), which is also much larger than expected.

We note that Keenan (1988) derived a much lower S VI 93.3 nm opacity value ($\tau_0 = 1.1 \times 10^{-4}$ at disk center) from a computation implying the cells of the network model of Gabriel (1976). However, while our value of $\tau_0$ seems to be too high, the level lines in Fig. 6 show that an opacity value $\tau_0 = 1.1 \times 10^{-4}$ would be too low: from this figure we expect that a value compatible with radiance measurements and realistic values of the temperature gradient would be in the range $5 \times 10^{-3}$ to $10^{-2}$.

### 5.2. Anomalous behavior of Na-like ions

Following work by Dupree (1972) for Li-like ions, Judge et al. (1995) report that standard DEM analysis fails for ions of the Li and Na isoelectronic sequences; in particular, for S VI (which is Na-like), Del Zanna et al. (2001) find that the atomic physics models underestimate the S VI 93.3 nm line radiance $E$ by a factor of 3. This fully explains the difference between our observation of $E$ and the value computed by CHIANTI (Table 1). However, this also means that where $G(T)$ from CHIANTI is used, as in Eq. (16), it presumably needs to be multiplied by 3. As a result, one can expect $\langle n_e \rangle_{\rm rms}$ to be lower by a factor 1.7, resulting in a filling factor of 415, which is poorer than our initial result.

The reasons for the anomalous behavior of these ions for $G(T)$, which could be linked to either ionization equilibrium or collisions, are still unknown. As a result, it is impossible to tell whether these reasons also produce an anomalous behavior of these ions for $K(T)$, hence in our measurements of opacities and estimates of densities: this could again reduce the filling factor.
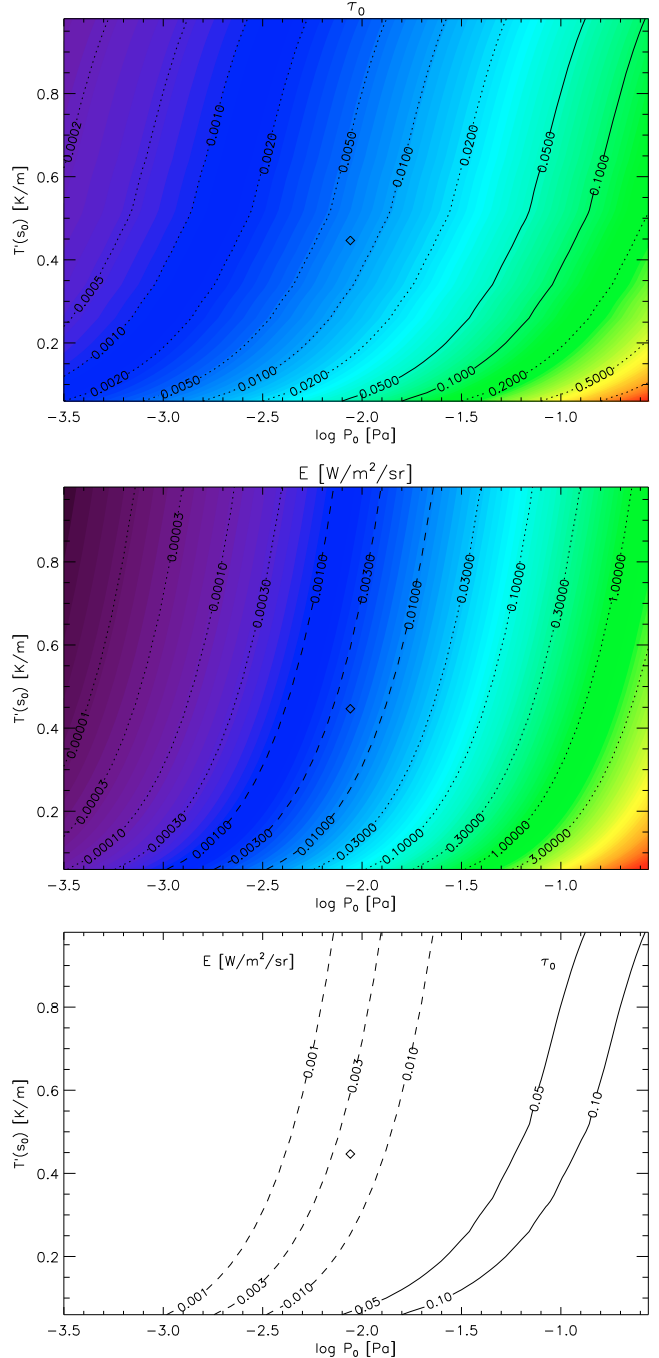


**Fig. 6.** S VI 93.3 nm opacity $\tau_0$ (*top panel*) and line radiance $E$ (*middle panel*) as a function of model parameters $P_0$ and $T'(s_0)$. The level lines close to our actual observations are shown as plain lines for $\tau_0$ and as dashed lines for $E$. *The bottom panel* reproduces these level lines together in the same plot. The parameters $(P_0, T'(s_0))$ estimated from the Avrett & Loeser (2008) model at $T = T_0$ are shown with the diamond sign on each plot.

### 5.3. Cell-and-network pattern

When analyzing our observations, we have not made the distinction between the network lanes and the cells of the chromospheric supergranulation. Here we try to evaluate the effect of the supergranular pattern on our measurements by using a 2D model emitting layer with a simple "paddle wheel" cell-and-network pattern: in polar coordinates $(r, \theta)$, the emitting layer is defined by $R_1 < r < R_2$; in the emitting layer, the network lanes are
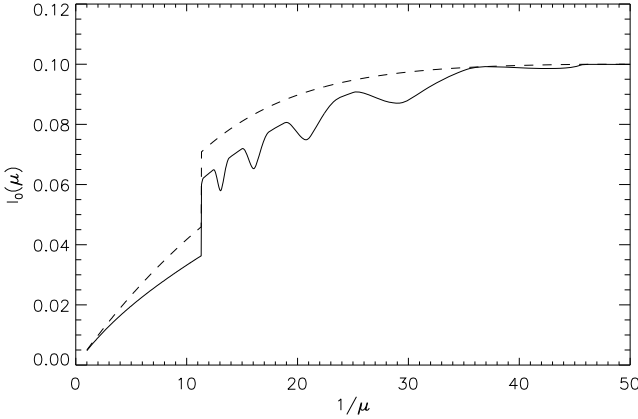
**Fig. 7.** Average spectral radiance at line center $I_0$ as a function of $1/\mu$ for a uniform layer (dashed line) and for a model layer with a simple cell-and-network pattern (plain line). Both models have the same average opacity and source function. The factor-2 jump at $1/\mu = 11.3$ corresponds to the limb of the opaque solar disk; the reference radius used to compute $\mu$ corresponds to the middle of the emitting layer. The oscillations are artefacts of the averaging process.

defined by $\theta \in [0, \delta\theta] \bmod \Delta\theta$ and the cells are in the other parts of the emitting layer, where $\Delta\theta$ is the pattern angular cell size (an integer fraction of $2\pi$) and $\delta\theta$ is the network lane angular size. The network lanes and cells are characterized by different (but uniform) source functions $S$, densities $n_{S\,VI}$, and absorption coefficients $k_{\nu_0}$. We then solve the radiative transfer equations for $\lambda_0$ along rays originating in infinity through the emitting layer to the observer.

Since the opacity is obtained by a simple integration of $k_{\nu_0} n_{S\,VI,i}$, the average line-of-sight opacity $t_0$ as a function of $\mu$ for the "paddle-wheel" pattern is the same as for a uniform layer with the same average $k_{\nu_0} n_{S\,VI,i}$. However, as seen in Fig. 7, still for the same average $S$ and $k_{\nu_0} n_{S\,VI,i}$, the effect of opacity (a decrease in intensity) is higher in the "paddle-wheel" case, in particular for intermediate values of $1/\mu$. As a result, neglecting the cell-and-network pattern of the true TR leads to overestimation of the opacity when using method A.

### 5.4. Roughness and fine structure

To explain the high values of opacity (as derived from their method A), Dumont et al. (1983) introduce the concept of roughness of the TR: since the TR plasma is not perfectly vertically stratified (there is some horizontal variation), method A leads to an overestimated value of $\tau_0$. This could reconcile the values obtained following our application of methods A and B.

We model the roughness of the transition region by incompressible vertical displacements of any given layer (at given optical depth) from its average vertical position, in the geometry shown in Fig. 8. The layer then forms an angle $\alpha$ with the horizontal and has still the same vertical thickness $ds$; the thickness along the LOS is $ds \cos\alpha / \cos(\theta + \alpha)$, as can be deduced from Fig. 8.

If we assume that $\theta + \alpha$ remains sufficiently small for the plane-parallel approximation to hold (and so that the LOS crosses one given layer only once), the opacity is

$$t_0 = \int n_e(s) K(T(s)) \frac{\cos\alpha \, ds}{\cos(\theta + \alpha)}. \qquad (24)$$
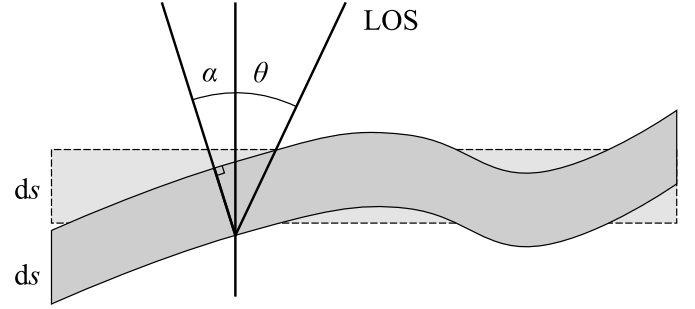


**Fig. 8.** Geometry of a TR layer (plain contour), displaced from its average position (dashed contour) while retaining its original vertical thickness $ds$, and locally forming an angle $\alpha$ with the average layer. The line-of-sight (LOS) forms an angle $\theta$ to the vertical (normal to the average layer).
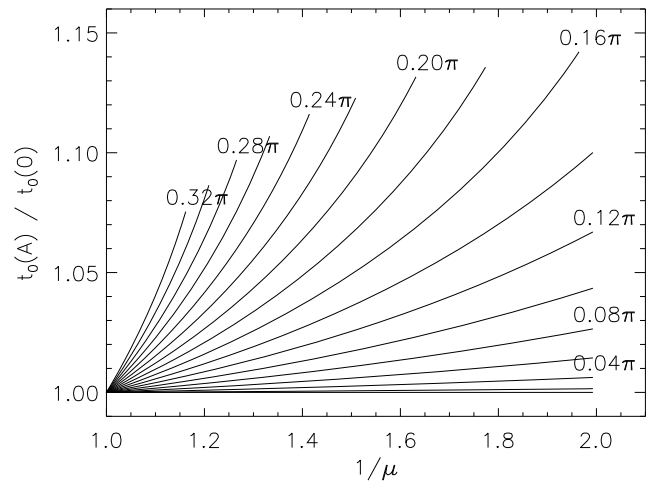


**Fig. 9.** Multiplicative coefficient to $t_0$ due to roughness, for different roughness parameters $A$.

The angle $\alpha$ is a random variable, with some given distribution $\Pr(\alpha)$. We compute the average of $t_0$ as a function of $\theta$ and of $\Pr(\alpha)$:

$$\langle t_0(\theta, \Pr(\alpha)) \rangle_\alpha = \iint n_e(s) K(T(s)) \frac{\cos\alpha \, ds}{\cos(\theta + \alpha)} \Pr(\alpha) \, d\alpha \qquad (25)$$

$$= \frac{\tau_0}{\mu} \left\langle \frac{\cos\theta \cos\alpha}{\cos(\theta + \alpha)} \right\rangle_\alpha \equiv \frac{\tau_0}{\mu} \beta(\theta, \Pr(\alpha)). \qquad (26)$$

The opacity $t_0 = \tau_0/\mu$ is corrected by the factor $\beta(\theta, \Pr(\alpha))$ defined in the previous equation. We recover $\beta = 1$ for $\Pr(\alpha) = \delta(\alpha)$, i.e., when there is no roughness.

We immediately see that $\beta = 1$ for $\theta = 0$, for any $\Pr(\alpha)$: roughness (as modeled here by incompressible vertical displacements) does not change the optical thickness at disk center. Nevertheless, the *estimate* of optical thickness at disk center from observations in Sect. 3.1 (method A of Dumont et al. 1983) is affected by this roughness effect.

Coming back to $\langle t_0 \rangle$, we take $\Pr(\alpha) = \cos^2(\pi\alpha/2A)/A$, and we compute $\beta$ numerically ($A$ represents the width of $\Pr(\alpha)$ and can be considered to be a quantitative measurement of the roughness). The results, shown in Fig. 9, indicate for example that the modeled roughness with $A = \pi/5$ increases the opacity by 9% at $1/\mu = 1.5$ (corresponding to $\theta = 45°$). This is a significant effect, and we can evaluate its influence on the estimate of $\tau_0$ in Sect. 3.1: in the theoretical profiles of $I_0(\mu)$ and $E(\mu)$ (Eqs. (2), (3)), $\tau_0/\mu$ needs to be replaced by $\tau_0/\mu \times \beta$. Since

$\beta > 1$ for a rough corona, this means that the value of $\tau_0$ determined from the fit of observed radiances to Eqs. (2), (3) is overestimated by a factor corresponding approximately to the mean value of $\beta$ for the fitting range.

In this way, we have estimated quantitatively the overestimation factor of $\tau_0$ by the method of Sect. 3.1, thus extending the qualitative discussion of roughness found in Dumont et al. (1983). This factor, of the order of 1.1 may seem modest, but one needs to remember that the fit for obtaining $\tau_0$ in Sect. 3.1 was completed for a wide range ($1/\mu$ from 1 to 5, or $\theta$ from 0 to 78 degrees) that our roughness model cannot reproduce entirely[7].

One can consider different roughness models that represent the strong inhomogeneity of the TR. For instance with a different and very peculiar roughness model, Pecker et al. (1988) obtained an overestimation factor of more than 10 under some conditions. This means that our values of $\tau_0$ may need to be decreased by a large factor because of a roughness effect.

Roughness models can be seen as simplified models of the fine structure of the TR, which is known to be heterogeneous on small scales. Indeed, in addition to the chromospheric network pattern that we modeled in Sect. 5.3, the TR contains parts of different structures, with different plasma properties, such as the base of large loops and coronal funnels, smaller loops (Dowdy et al. 1986; Peter 2001), and spicules. Furthermore, the loops themselves are likely to consist of strands, which can be heated independently (Cargill & Klimchuk 2004; Parenti et al. 2006). The magnetic field in these structures inhibits perpendicular transport, and as a consequence the horizontal inhomogeneities are not smoothed out efficiently.

## 6. Conclusion

We have derived the average electron density in the TR from the opacity $\tau_0$ of the S VI 93.3 nm line, which was obtained by three different methods from observations of the full Sun: center-to-limb variation in radiance, center-to-limb ratios of radiance and line width, and radiance ratio of the 93.3−94.4 nm doublet. Assuming a spherically symmetric plane-parallel layer of constant source function, we found a S VI 93.3 nm opacity of the order of 0.05. The derived average electron density is of the order of $2.4 \times 10^{16}$ m$^{-3}$.

We have then used the line radiance (by an EM method) to derive the rms average electron density in the S VI 93.3 nm-emitting region and obtained $2.0 \times 10^{15}$ m$^{-3}$. This corresponds to a total pressure of $10^{-2}$ Pa, slightly higher than the range of pressures found by Dumont et al. (1983) (1.3 to $6.3 \times 10^{-3}$ Pa, as deduced from their Sect. 4.2), but lower than the value given in Mariska (1993) ($2 \times 10^{-2}$ Pa).

The average electron densities obtained from these methods (opacity on the one hand, radiance on the other hand) are incompatible, as can be seen either from a direct comparison of the values of $\langle n_e \rangle$ and $\langle n_e^2 \rangle$ for a given thickness $\Delta s$ of a uniform emitting layer, or by computing the $\Delta s$ that would reconcile the measurements of $\langle n_e \rangle \Delta s$ and $\langle n_e^2 \rangle \Delta s$. Furthermore, we have seen that the density obtained from the opacity method is also incompatible with standard DEMs of the Quiet Sun (see Sect. 4.2) and

with semi-empirical models of the temperature and density profiles in the TR (see Sect. 5.1.2).

We investigated several possible sources of biases in the determination of $\tau_0$: the approximation of a constant temperature in the S VI emitting layer, the anomalous behavior of the S VI ion, the chromospheric network pattern, and the roughness of the TR. Some of these could help explain partly the discrepancy between the average densities deduced from opacities and from radiances, but there is still a long way to go to fully understand this discrepancy and to reconcile the measurements. At this stage, we can only encourage colleagues to look for similar discrepancies in lines formed around $\log T = 5.3$ (like C IV and O VI), Na-like and not Na-like, and to repeat similar S VI center-to-limb measurements.

In Sect. 5.1.2, we tried to combine opacity and radiance information to compute the gradient of temperature. This appeared to be impossible (if restricting ourselves to a realistic range of parameters) because of the above-mentioned incompatibility. We have estimated that a value $\tau_0$ of the S VI 93.3 nm opacity compatible with radiance measurements and with realistic values of the temperature gradient should be in the range $5 \times 10^{-3}$ to $10^{-2}$.

In spite of the difficulties that we met, we still think that the combination of opacity and radiance information should be a powerful tool for investigating the thermodynamic properties and the fine structure of the TR. For instance, the excess opacity derived from observations and a plane-parallel model could be used to evaluate models of roughness and the fine structure of the TR. Clearly, progress in modelling the radiative output of the complex structure of the TR needs to be made to achieve this.

## Appendix A: About the filling factor

In this paper, we have defined the filling factor as

$$f = \frac{\langle n_e \rangle^2}{\langle n_e^2 \rangle}, \tag{A.1}$$

while it is usually inferred from solar observations (e.g. Judge 2000; Klimchuk & Cargill 2001) to be

$$f = \frac{EM}{\Delta s \, n_0^2}, \tag{A.2}$$

where $EM$ is the emission measure, $\Delta s$ is the thickness of the plasma layer, and $n_0$ is the electron density (usually determined from line ratios) *in the non-void parts of the plasma layer*.

It may seem surprising that the $EM$ is in the numerator of this second expression, while it provides an estimate for $\langle n_e^2 \rangle$, which appears in the denominator of the first expression. However, we can show that both expressions, despite looking very different, actually provide the same result for a given plasma.

We assume a plasma with a differential distribution $\xi(n_e, T)$ for the density and temperature, i.e., $\xi(n_e, T) \, dn_e \, dT$ is the proportion of any given volume occupied by plasma at a density between $n_e$ and $n_e + dn_e$, and a temperature between $T$ and $T + dT$.

---

[7] For high values of the Pr($\alpha$) width $A$, the correction factor $\beta$ cannot be computed for high values of $1/\mu$ (high angles $\theta$) because the values of $\alpha$ in the wings of Pr($\alpha$) fall in the range where $|\theta + \alpha| \not\ll \pi/2$: the plane-parallel approximation is no longer valid. This explains the limited range of the $\beta(1/\mu)$ curves in Fig. 9.

The contributions to both the line radiance $E$ and the opacity at line center $\tau_0$ from a volume $V$ with this plasma distribution are

$$\frac{E}{V} = \iint n_e^2 G(n_e, T) \, \xi(n_e, T) \, dn_e \, dT \tag{A.3}$$

$$\frac{\tau_0}{V} = \iint n_e K(n_e, T) \, \xi(n_e, T) \, dn_e \, dT \tag{A.4}$$

with the usual notations of our article.

The usual assumption (e.g. Judge 2000) is that $G(T, n_e)$ "selects" a narrow range of temperatures around $T = T_{max}$ and does not depend on $n_e$, i.e., $G(n_e, T) \approx \tilde{G}(T_{max}) \, \delta(T - T_{max})$. Similarly, we can consider that $K(n_e, T) \approx \tilde{K}(T_{max}) \, \delta(T - T_{max})$. Then

$$\frac{E}{V} \approx \tilde{G}(T_{max}) \int n_e^2 \xi(n_e, T_{max}) \, dn_e = \tilde{G}(T_{max}) \langle n_e^2 \rangle_{T=T_{max}} \tag{A.5}$$

$$\frac{\tau_0}{V} \approx \tilde{K}(T_{max}) \int n_e \xi(n_e, T_{max}) \, dn_e = \tilde{K}(T_{max}) \langle n_e \rangle_{T=T_{max}}. \tag{A.6}$$

Following Judge (2000) and for the assumption $G(n_e, T) = \hat{G}(n_e, T_{max}) \, \delta(T - T_{max})$, the line ratio $R_{ij} = E_i/E_j$ is

$$R_{ij} = \frac{E_i}{E_j} = \frac{\iint n_e^2 G_i(n_e, T) \, \xi(n_e, T) \, dn_e \, dT}{\iint n_e^2 G_j(n_e, T) \, \xi(n_e, T) \, dn_e \, dT} \tag{A.7}$$

$$\approx \frac{\int n_e^2 \hat{G}_i(n_e, T_{max}) \, \xi(n_e, T_{max}) \, dn_e}{\int n_e^2 \hat{G}_j(n_e, T_{max}) \, \xi(n_e, T_{max}) \, dn_e}. \tag{A.8}$$

When homogeneity is assumed, i.e., $\xi(n_e, T) = \delta(n_e - n_0) \, \tilde{\xi}(T)$, this becomes

$$R_{ij} \approx \frac{n_0^2 G_i(n_0, T_{max}) \, \tilde{\xi}(T_{max})}{n_0^2 G_j(n_0, T_{max}) \, \tilde{\xi}(T_{max})} = \frac{G_i(n_0, T_{max})}{G_j(n_0, T_{max})} \equiv g_{ij}(n_0) \tag{A.9}$$

and inverting this function allows us to recover $n_0$ from the observed value of $R_{ij}$.

The fundamental point is that $R_{ij}$ does not depend on the proportion $f$ (the filling factor) of the volume occupied by the plasma, and $n_0$ is the density in the non-void region only. For example, for $\xi_f(n_e, T)$ defined by $f \delta(n_e - n_0) + (1 - f) \delta(n_e)$, the line ratio $R_{ij}$ is $g_{ij}(n_0)$, which is independent of $f$, while $\langle n_e^2 \rangle_{T=T_{max}}$

determined from $E/V$ would be $f n_0^2$, and $\langle n_e \rangle_{T=T_{max}}$ determined from $\tau_0/V$ would be $f n_0$. In this case, one can see that $f$ can (equivalently) either be recovered from

$$\frac{\langle n_e^2 \rangle_{T=T_{max}}}{(n_0)^2} = \frac{(f n_0^2)}{(n_0)^2} = f \tag{A.10}$$

(corresponding to Judge 2000) or from

$$\frac{\langle n_e \rangle_{T=T_{max}}^2}{\langle n_e^2 \rangle_{T=T_{max}}} = \frac{(f n_0)^2}{(f n_0^2)} = f \tag{A.11}$$

(corresponding to our method).

## References

Avrett, E. H., & Loeser, R. 2008, ApJS, 175, 229
Buchlin, E., Vial, J.-C., & Lemaire, P. 2006, A&A, 451, 1091
Cargill, P. J., & Klimchuk, J. A. 2004, ApJ, 605, 911
Curdt, W., Brekke, P., Feldman, U., et al. 2001, A&A, 375, 591
Del Zanna, G., Bromage, B. J. I., & Mason, H. E. 2001, in Joint SOHO/ACE workshop, Solar and Galactic Composition, ed. R. F. Wimmer-Schweingruber, AIP Conf. Ser., 598, 59
Dere, K. P., Landi, E., Mason, H. E., Monsignori Fossi, B. C., & Young, P. 1997, A&AS, 125, 149
Dowdy, J. F., Rabin, D., & Moore, R. L. 1986, Sol. Phys., 105, 35
Dumont, S., Pecker, J.-C., Mouradian, Z., Vial, J.-C., & Chipman, E. 1983, Sol. Phys., 83, 27
Dupree, A. K. 1972, ApJ, 178, 527
Gabriel, A. 1976, R. Soc. London Phil. Trans. Ser. A, 281, 339
Judge, P. G. 2000, ApJ, 531, 585
Judge, P. G., Woods, T. N., Brekke, P., & Rottman, G. J. 1995, ApJ, 455, L85
Keenan, F. P. 1988, Sol. Phys., 116, 279
Klimchuk, J. A., & Cargill, P. J. 2001, ApJ, 553, 440
Landi, E., Del Zanna, G., Young, P. R., et al. 2006, ApJS, 162, 261
Mariska, J. T. 1993, The Solar Transition Region (Cambridge University Press)
Mason, H. E. 1998, in Space Solar Physics: Theoretical and Observational Issues in the Context of the SOHO Mission, ed. J. C. Vial, K. Bocchialini, & P. Boumier, Lecture Notes in Physics (Berlin: Springer Verlag), 507, 143
Parenti, S., Buchlin, E., Cargill, P. J., Galtier, S., & Vial, J.-C. 2006, ApJ, 651, 1219
Pecker, J.-C., Dumont, S., & Mouradian, Z. 1988, A&A, 196, 269
Peter, H. 1999, ApJ, 516, 490
Peter, H. 2001, A&A, 374, 1108
Peter, H., & Judge, P. G. 1999, ApJ, 522, 1148
Wilhelm, K., Curdt, W., Marsch, E., et al. 1995, Sol. Phys., 162, 189